# Observation of an amplitudelike mode in the excitonic insulator $Ta_2Pd_3Te_5$

Y.-S. Choi [1], Dirk Wulferding [2,*], Raju Kalaivanan [3], Rajesh Kumar Ulaganathan [4], Raman Sankar [3,†] and Kwang-Yong Choi [1,‡]

[1]*Department of Physics, Sungkyunkwan University, Suwon 16419, Republic of Korea*
[2]*Department of Physics and Astronomy, Sejong University, Seoul 05006 Republic of Korea*
[3]*Institute of Physics, Academia Sinica, Nankang, Taipei 11529, Taiwan*
[4]*Centre for Nanotechnology, Indian Institute of Technology, Roorkee, India*

(Received 7 September 2025; accepted 19 May 2026; published 10 June 2026; corrected 26 June 2026)

The excitonic insulator candidate $Ta_2Pd_3Te_5$ has emerged as a promising platform to explore macroscopic quantum condensation and its collective excitations. Using polarization-resolved Raman spectroscopy, we identify a symmetry-selective electronic mode that softens and undergoes linewidth renormalization across the characteristic temperature $T^* \sim 100$ K. This mode, most prominent in the $B_{3g}$ channel, is assigned to vestigial collective excitations associated with excitonic correlations, as evidenced by its order-parameter-like temperature evolution and symmetry dependence. In parallel, a damped Drude-like response exhibits a suppressed scattering rate and maximum intensity at $T^*$, while phonon intensities display symmetry-dependent anomalies, signaling anisotropic band reconstructions and the spontaneous opening of a collective condensation gap. These observations provide compelling spectroscopic evidence for collective amplitude excitations in $Ta_2Pd_3Te_5$, establishing this material as a bulk excitonic insulator.

DOI: 10.1103/2swg-p1pn

## I. INTRODUCTION

Since its theoretical inception in the 1960s, the quest for excitonic insulators (EIs) in bulk crystals has constituted a major challenge in quantum materials research [1]. In the EI phase, electrons and holes spontaneously bind into excitons, forming a macroscopic condensate below a critical temperature. This symmetry-broken insulating phase is stabilized by strong Coulomb interactions, manifests itself as a spontaneous hybridization gap at the Fermi level, and entails collective amplitude excitations of the excitonic order parameter [2–9].

In bulk materials, however, the unambiguous identification of this elusive state is complicated by the intricate interplay of electronic, lattice, spin, and orbital degrees of freedom. In many candidate systems, excitonic correlations are intimately intertwined with competing instabilities such as charge density wave (CDW) and phonon-driven structural distortions. For instance, in 1T-$TiSe_2$, the putative excitonic instability is strongly linked to CDW order [10–15]. Similarly, in the most widely studied EI candidate $Ta_2NiSe_5$, a semimetal-to-semiconductor transition occurs at $T_C = 328$ K, initially ascribed to exciton condensation [16–28]. Subsequent experiments, however, established that this electronic transition is accompanied by an orthorhombic-to-monoclinic structure transition, complicating clear disentanglement of electronic and lattice contributions.

Amid the long-standing search for bulk EIs, the layered van der Waals compound $Ta_2Pd_3Te_5$ (*Pnma* space group), structurally analogous to the high-symmetry phase of $Ta_2NiSe_5$, has emerged as a promising contender [29–41]. In its crystal structure, $Ta_2Pd_3Te_5$ monolayers are stacked along the $a$ axis, within which quasi-one-dimensional Ta-Te and Pd-Te chains extend along the $b$ axis [see Fig. 1(a)]. First-principles calculations predict that its monolayer hosts an EI state, driven by strong electron-hole attraction in a nearly zero-gap semimetallic band structure [31]. Experimentally, resistivity and angle-resolved photoemission spectroscopy (ARPES) attest to a metal-insulator transition (MIT) from Dirac semimetal-like to semiconducting behavior near $T_{MIT} \approx 365$ K [37,38]. At lower temperatures, scanning tunneling microscopy (STM) reveals the emergence of a temperature-dependent gap and in-gap topological edge states below $T^* = 100$ K [39]. Unlike 1T-$TiSe_2$ and $Ta_2NiSe_5$, this insulating gap in $Ta_2Pd_3Te_5$ appears to originate primarily from electron-hole Coulomb interactions rather than single-particle band reconstructions or lattice distortions. As such, this compound offers an excellent setting to investigate the fundamental mechanisms underpinning excitonic condensation through the detection of collective charge excitations.

In this paper, we employ polarization-resolved Raman spectroscopy to probe the intriguing landscape of excitonic condensation in $Ta_2Pd_3Te_5$. Our spectroscopic measurements resolve an amplitudelike mode arising from the formation of a coherent excitonic condensate below $T^* = 100$ K, preceded by a broad fluctuation regime extending between $T_{MIT}$ and $T^*$.

*Contact author: d.wulferding@sejong.ac.kr
†Contact author: sankarndf@gmail.com
‡Contact author: choisky99@skku.edu

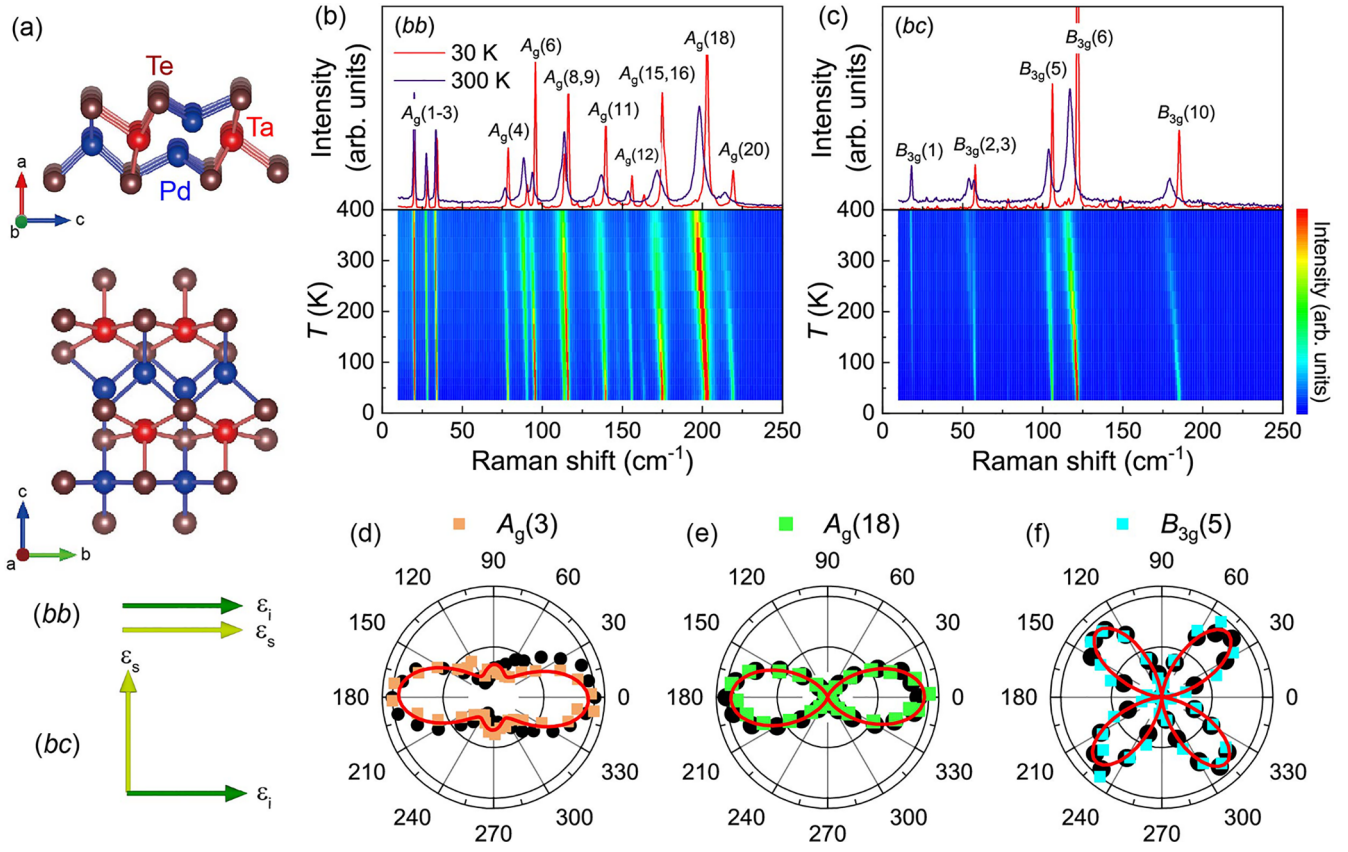


FIG. 1. (a) Crystal structure of $Ta_2Pd_3Te_5$ comprising chains running along the $b$ axis. The arrows represent the polarization configurations. (b), (c) As-measured Raman spectra of $Ta_2Pd_3Te_5$ at $T = 30$ K and 300 in the ($bb$) and ($bc$) polarization configurations, respectively, with phonon modes labeled according to their symmetries. Corresponding color maps of Raman intensity vs Raman shift as a function of temperature ($T = 30$–390 K) for the ($bb$) and ($bc$) configurations, corresponding to the $A_g$ and $B_{3g}$ symmetry channels. (d)–(f) Polar plots of the normalized Raman intensity for selected $A_g(3)$, $A_g(18)$, and $B_{3g}(5)$ modes. Colored square (black circles) symbols correspond to the 30 K (300 K) data. Red solid lines are theoretical fits based on the Raman tensors for the $D_{2h}$ point group.

These results underscore the potential implications for collective excitations in excitonic insulator candidate materials.

## II. EXPERIMENTAL DETAILS

High-quality single crystals of $Ta_2Pd_3Te_5$ were grown via a slow cooling process. Initially, stoichiometric amounts of high-purity Ta slug (99.999%), Pd powder (99.999%), and Te slug (99.999%) were mixed and sealed in a carbon-coated silica ampoule under high vacuum. The mixture was heated at 400 and 700 °C for 24 h each, with intermediate grinding in an argon-filled glove box. The resulting polycrystalline powders were sealed in a conical quartz ampoule ($\sim 10^{-3}$ Torr), heated at 750 °C for 24 h, and then cooled to 550 °C at a rate of 1 °C/min.

Polarization- and temperature-dependent low-frequency ($8-500\,\mathrm{cm}^{-1}$) Raman spectra were recorded using 660 nm laser (Cobolt) focused through a 40× microscope objective onto the sample surface with a spot diameter of less than 2 μm and a laser power below $P = 0.5$ mW. The sample was mounted into a He-flow microscope-type cryostat (Oxford MicroStat). Raman-scattered signals were dispersed through a Princeton Instruments TriVista777 spectrometer onto a PyLoN eXcelon charge-coupled device detector.

## III. RESULTS

### A. Temperature and angle dependence of phonon Raman spectra

To assess the role of electron-phonon coupling in excitonic gap formation, we first examine possible lattice anomalies. Figures 1(b) and 1(c) present Raman spectra of $Ta_2Pd_3Te_5$ measured at $T = 300$ and 30 K in the ($bb$) and ($bc$) polarizations, respectively, with the corresponding scattering geometries depicted in the bottom of Fig. 1(a).

According to factor-group analysis for the orthorhombic space group $Pnma$, 60 Raman-active phonon modes are expected: $20A_g(aa, bb, cc) + 10B_{1g}(ab) + 20B_{2g}(ac) + 10B_{3g}(bc)$. Under the present scattering geometries, all symmetry-allowed $20A_g$ and $10B_{3g}$ modes are observed. For clarity, only prominent modes are labeled by their symmetries in Figs. 1(b) and 1(c), while the complete mode assignment is provided in the Supplemental Material [42]. Notably, temperature-dependent Raman intensity maps reveal that several phonon modes become more distinctly resolved upon cooling to 30 K. These phonon anomalies arise from enhanced Raman susceptibility due to weak lattice distortions that deviate from the orthorhombic symmetry. Notably, $Ta_2Pd_3Te_5$ exhibits no soft-mode-like behavior, such as

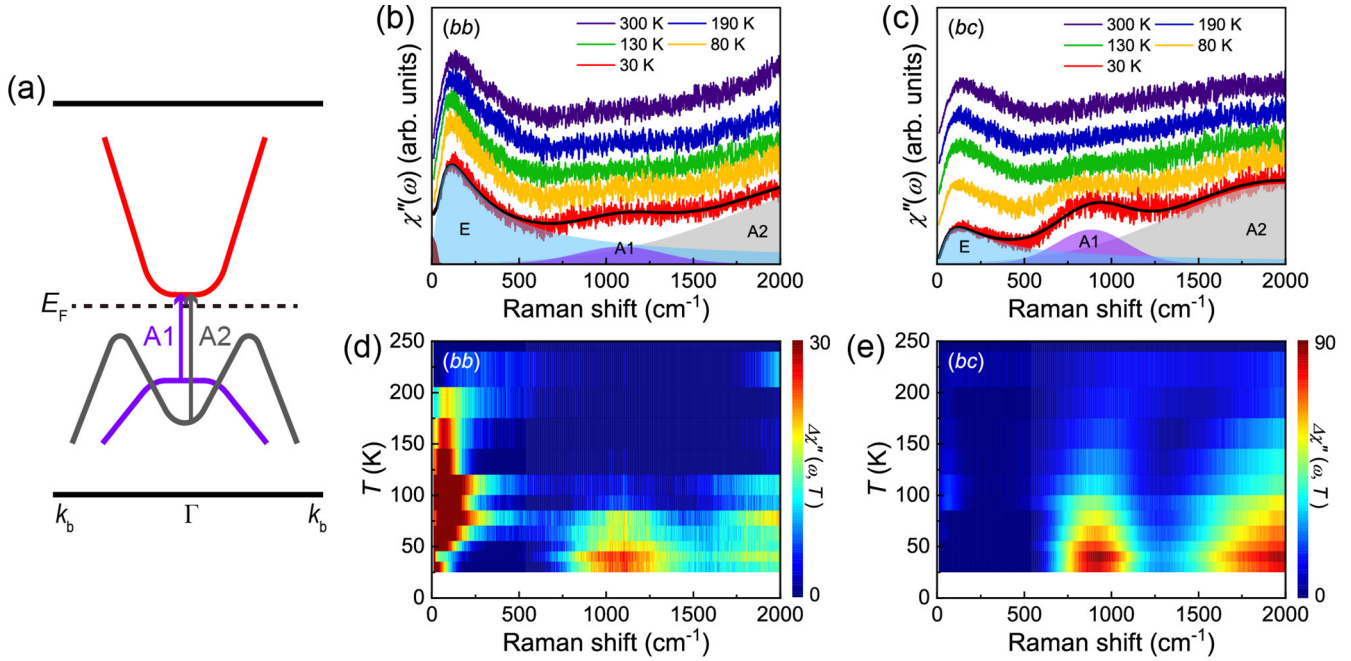


FIG. 2. (a) Sketch of A1 and A2 excitation processes. (b), (c) Raman susceptibility $\chi''(\omega)$ measured in the ($bb$) and ($bc$) polarization channels at selected temperatures from 300 to 30 K. The electronic response is decomposed into multiple components: a collision-dominated continuum and two amplitudelike modes (A1: purple; A2: gray). The solid lines are fits to the sum of the damped Drude response and two Gaussian components as detailed in the main text. In the ($bb$) channel, an additional low-energy background feature (wine colored) emerges. (d), (e) Color maps of the differential Raman response, $\Delta\chi''(\omega, T) = \chi''(\omega, T) - \chi''(\omega, T = 260\,\mathrm{K})$, for the ($bb$) and ($bc$) polarization geometries, respectively. A marked enhancement of spectral weight associated with the A1 and A2 modes appears below approximately $T^* = 100\,\mathrm{K}$.

substantial phonon softening or linewidth anomalies, across $T_{\mathrm{MIT}}$. Rather, the dominant feature is a change in phonon intensity, which often stems from electronic band structure modifications. Lattice distortion is therefore unlikely to be the primary driver of the insulating transition.

We next turn to angle-resolved Raman spectra at 300 and 30 K. Figures 1(d)–1(f) display polar plots of the normalized Raman intensities for selected $A_g(3)$, $A_g(18)$, and $B_{3g}(5)$ modes (see the Supplemental Material for more phonon modes [42]). For the $D_{2h}$ point group, the angular dependencies follow the characteristic twofold or fourfold periodicities: $I_{A_g} = (|b|\cos^2\theta\cos(\phi_c - \phi_b) + |c|\sin^2\theta)^2 + |b|^2\cos^4\theta\sin^2(\phi_c - \phi_b)$ and $I_{B_{3g}} = |f|^2\sin^2 2\theta$, where $\theta$ denotes the angle relative to the $b$ axis and $\phi_c - \phi_b$ is the phase difference between the $b$ and $c$ components of the Raman tensor. Remarkably, no signatures of rotational symmetry breaking are detected down to 30 K. As detailed in the Supplemental Material [42], no thermal anomalies are observed either. These results are consistent with earlier reports that identified only subtle lattice distortions in electron diffraction, but none in x-ray or thermodynamic probes [37,38].

### B. Electronic Raman responses

We inspect the electronic Raman response and associated low-energy excitations, measured up to the spectral range of 2000 cm$^{-1}$. In general, the electronic Raman intensity is given by $I_R(\omega) \propto \sum_k |\gamma(k)|^2\delta(\omega - E(k))$, where the Raman vertex $\gamma(k)$ weights electronic transitions according to the specific polarization geometry [43].

In semimetals, the electronic Raman spectrum involves intraband scattering featuring a Drude-like response. This collision-dominated response originates from the scattering of itinerant charge carriers off impurities, phonons, or other degrees of freedom and is effectively modeled using a damped Drude-like susceptibility, $\chi''_{\mathrm{CD}}(\omega) = B\omega/(\omega^2 + \Gamma^2)$, with the symmetry-dependent amplitude $B$ and carrier scattering rate $\Gamma$ [44]. In addition to this Drude component, interband scattering transitions between the valence and conduction bands, particularly when a finite single-particle gap is present, can contribute, as schematically illustrated in Fig. 2(a).

Figures 2(b) and 2(c) present the representative Raman response $\chi''(\omega, T)$, obtained from the raw Raman data $I_R(\omega, T)$ via the relation $I_R(\omega, T) = [1 + n(\omega, T)]\chi''(\omega, T)$, where $n(\omega, T)$ is the Bose factor. We note that the ($bb$) and ($bc$) polarization configurations probe excitations in the $A_g$ (fully symmetric) and $B_{3g}$ ($d_{yz}$-like quadrupolar) channels, respectively. Phonon modes were removed by Lorentzian fitting. At high temperatures, $\chi''(\omega, T)$ is dominated by a damped Drude-like component (labeled "E") at low frequencies, along with a weakly increasing background at higher frequencies. As the temperature is lowered, additional distinct electronic features become progressively discernible. In the ($bb$) polarization, two broad peaks appear at approximately $\omega_{A1}^{(bb)} \approx 1086$ and $\omega_{A2}^{(bb)} \geqslant 2000$ cm$^{-1}$. Accordingly, the electronic Raman response $\chi''(\omega, T)$ is modeled as the sum of a collision-dominated contribution and two

Gaussian profiles $\chi''_G(\omega)$ (labeled "A1" and "A2"), as indicated by the color-shaded areas. The solid lines represent fits to $\chi''(\omega) = \chi''_{\rm CD}(\omega) + \sum_{i=1}^{2} \chi''_{G_i}(\omega)$. The fitting details and the extracted parameters are provided in the Supplemental Material [42]. We further note that in the (*bc*) polarization, these high-frequency peaks grow in intensity with decreasing temperature relative to the E continuum, while shifting to lower energies: $\omega_{A1}^{(bc)} \approx 975$ cm$^{-1}$ and $\omega_{A2}^{(bc)} \approx 1900$ cm$^{-1}$. The polarization dependence of the A1 and A2 energies is attributed to the anisotropy of the excitonic gap combined with the symmetry-selective Raman vertex. In the $A_g$ (*bb*) configuration, $\gamma(k)$ predominantly couples to regions with maximal band curvature, thereby sampling the largest excitonic gap. In contrast, the $B_{3g}$ (*bc*) channel involves an antisymmetric form factor that probes different momentum regions, where the effective gap is smaller.

To isolate the emergent spectral features from the broad continuum, we subtract the Raman response $\chi''(\omega, T)$ by the $T = 260$ K spectrum. The resulting differential spectra, $\Delta\chi''(\omega, T) = \chi''(\omega, T) - \chi''(\omega, T = 260\ \text{K})$, are plotted in Figs. 2(d) and 2(e). In the (*bb*) channel, a quasielastic scattering develops, reaching maximum intensity near $T^* \sim 100$ K, below which the spectral weight of the A1 and A2 excitations is noticeably enhanced. In sharp contrast, in the (*bc*) channel, the A1 excitation is already visible at 260 K and gradually intensifies upon cooling through $T^*$. Concurrently, the A2 feature steadily grows in intensity and broadens with decreasing temperature. The symmetry-selective enhancement and distinct temperature evolution of these features are incompatible with trivial interband transitions. In particular, the rapid suppression of the A1 and A2 peaks above $T^*$, despite their characteristic energies on the order of 1000 K, attests to the thermal decoherence of these collective excitations and the strong renormalization of the electronic band structure.

### C. Amplitudelike modes

On this basis, we infer that the A1 and A2 peaks involve gapped excitations between hybridized bands created or reconstructed via exciton condensation. Several observations support the interpretation of collective excitonic order.

First, theoretical calculations show that the excitonic order parameter transforms according to the $B_{3g}$ irreducible representation of the $D_{2h}$ space group [23]. Accordingly, the A1 excitation, pronounced in the (*bc*) channel, is associated with amplitude (Higgs-like) modes corresponding to coherent electron-hole pair hopping between Ta and Pd chains [see the schematic in Fig. 2(a)]. Regarding the A2 excitation, its character as an amplitude mode is less obvious owing to its broader spectral profile and hybridization with other bands. Second, optical conductivity measurements reveal several sharp features at low temperatures: $\alpha = 620$ cm$^{-1}$, $\beta = 1100$ cm$^{-1}$, and $\gamma = 1950$ cm$^{-1}$ along the *b* axis and $\alpha = 900$ cm$^{-1}$ and $\gamma = 2100$ cm$^{-1}$ along the *c* axis [45]. These emergent peaks are interpreted in terms of signatures of flat bands induced by exciton condensation. Their close energetic correspondence with the Raman features signifies the condensation of the A1's spectral weight into a collective excitonic mode, distinct from the interband continuum.

Shown in Figs. 3(a) and 3(b) is the temperature evolution of Raman intensities for selected $A_g$ and $B_{3g}$ phonons. Since the phonon Raman intensity is proportional to the derivative of the electronic susceptibility with respect to normal-mode displacements, it reflects band renormalization across excitonic instabilities. Overall, the $A_g$ modes exhibit a monotonic intensity enhancement upon cooling through ∼150 K. In contrast, the $B_{3g}$ phonons exhibit more intriguing behavior: The $B_{3g}(1)$ mode grows in intensity down to 240 K before leveling off and eventually fading away below $T^*$, while the $B_{3g}(2)$ mode steadily weakens on cooling below 240 K and almost disappears around $T^*$. This symmetry-dependent evolution points to symmetry-selective electron-phonon coupling, with the strongest effects observed in the $B_{3g}$ channel (see below for further discussion).

We now analyze the damped Drude-like response. In Figs. 3(c) and 3(d), we plot the temperature dependence of the amplitude $B$ and scattering rate $\Gamma$. With lowering temperature, $B(T)$ increases gradually with a slight slope change around $T_{\rm MIT}$, reaches a maximum near $T^*$, and then drops sharply. Remarkably, this trend mirrors the thermal evolution of the $B_{3g}(1)$ mode [pink triangles in Fig. 3(b)]. This coincidence indicates that the $B_{3g}(1)$ lattice vibration is closely tied to the underlying excitonic instability, which transforms according to the $B_{3g}$ irreducible representation [23]. On the other hand, $\Gamma(T)$ decreases continuously with cooling and saturates below $T^*$. The subtle anomaly at $T_{\rm MIT}$ and the pronounced anomaly at $T^*$ suggest that competing interactions and multiband hybridizations hinder the full development of coherent collective modes even though the insulating gap has already opened below $T_{\rm MIT}$.

We next examine the high-energy excitation. Figures 3(e) and 3(f) present the temperature evolution of the A1 peak energy and linewidth in the (*bc*) channel. Reliable analysis in the (*bb*) channel is precluded by the weak A1 intensity, while the A2 feature is too broad. As the temperature is lowered from 240 K toward $T^*$, the A1 mode undergoes pronounced softening, followed by slight hardening for $T < T^*$. As shown in the inset of Fig. 3(e), the A1 mode energy follows an order-parameter-like increase below $T^*$. Nonetheless, the observed hardening of approximately 40 cm$^{-1}$ below $T^*$ is roughly an order of magnitude smaller than the softening starting at 260 K. Given that the A1 excitation overlaps with both the A2 mode and the Drude-like response, as shown in Figs. 2(b) and 2(c), the anticipated amplitude mode appears substantially damped and renormalized, despite the opening of the insulating gap. Similarly, its linewidth decreases modestly with decreasing temperature to 240 K and then narrows substantially on approaching $T^*$ and finally shows a slight upturn below $T^*$. The observed hardening and broadening cannot be readily explained within the behavior based on a simple band structure reconfiguration, where the energy gap would evolve monotonically below $T_{\rm MIT}$. Rather, the $T^*$ anomaly is reminiscent of the coherent gap evolution observed by STM measurements [39].

## IV. DISCUSSION AND SUMMARY

Our temperature- and polarization-dependent Raman spectroscopic study of $Ta_2Pd_3Te_5$ enables mapping out a

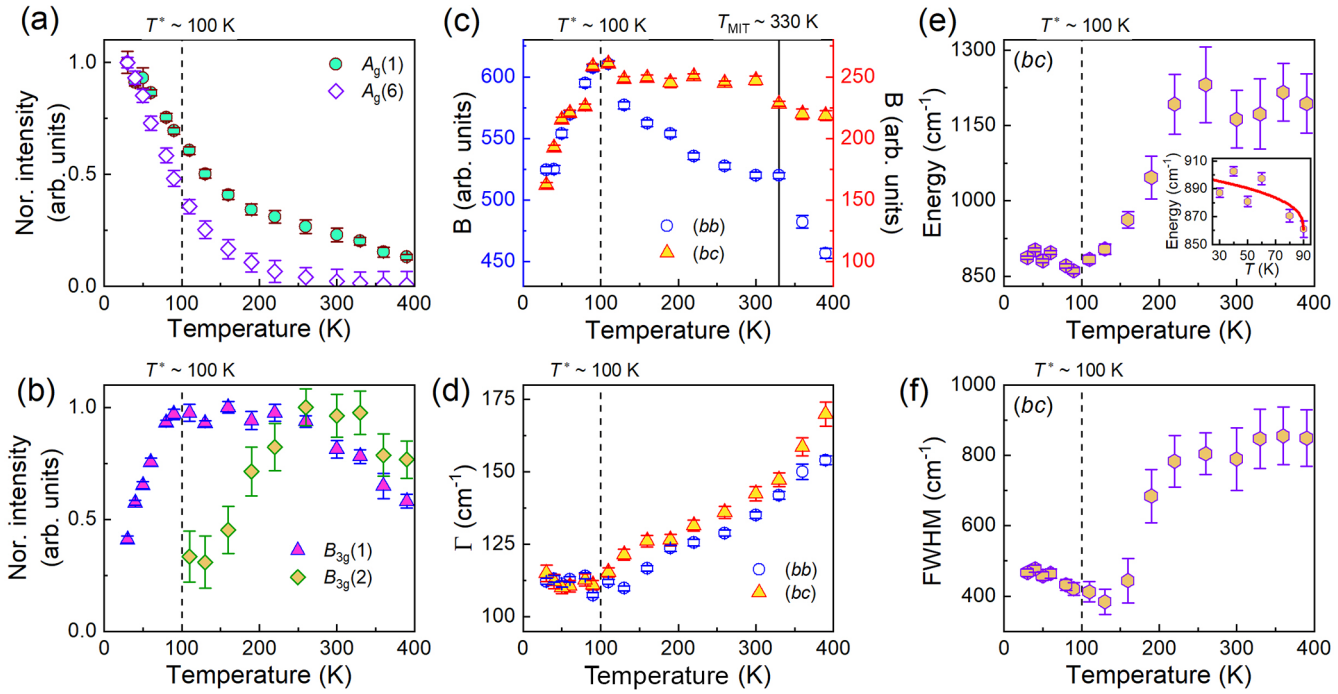


FIG. 3. Thermal evolution of Raman intensities for (a) $A_g$ phonons and (b) $B_{3g}$ phonons. (c) Amplitude of the collision-dominated scattering continuum for the (*bb*) (blue circles) and (*bc*) (pink triangles) polarization geometries. (d) Scattering rate $\Gamma$ of the Drude-like continuum as a function of temperature for both polarization channels. The vertical dashed lines mark the characteristic temperature ($T^* \approx 100$ K) below which the amplitudelike modes emerge. (e) Energy and (f) FWHM of the amplitudelike excitation A1 in the (*bc*) channel, extracted from Gaussian fits.

comprehensive landscape of low-energy phononic and electronic excitations, providing fresh insights into the nature of excitonic condensation.

Unlike lattice-driven transitions in related EI systems such as $Ta_2NiSe_5$ and 1T-$TiSe_2$ [25,46], only a subtle structural transition accompanies the insulator-metal transition. The absence of characteristic soft-phonon behavior is inconsistent with a lattice-driven scenario. Furthermore, the prominent anomalies in the $B_{3g}$ phonons underscore their symmetry-selective coupling to band reconstructions driven by excitonic hybridization. The Drude-like continuum provides complementary information about this electronic reorganization. Its amplitude $B(T)$ exhibits a pronounced maximum at $T^*$, while the scattering rate $\Gamma(T)$ forms a minimum at the similar temperature. This is contrasted by only weak anomalies at $T_{\mathrm{MIT}}$. These results indicate that the exciton condensation becomes coherent only upon further cooling to $T^*$, well below $T_{\mathrm{MIT}}$. Noteworthy is that while resistivity and ARPES data reveal the onset of a partial gap opening across the Brillouin zone below $T_{\mathrm{MIT}}$, STM measurements resolve a fully coherent energy gap only below $T^* \approx 100$ K [37–39]. These distinct responses allude to a crossover regime in the temperature range $T^* < T < T_{\mathrm{MIT}}$, where excitonic correlations manifest as incoherent excitons. Raman spectroscopy, as a two-particle probe of charge fluctuations at the Brillouin zone center ($q \approx 0$), is sensitive to the long-wavelength collective mode that develops below $T^*$ [43].

In this crossover regime, the amplitudelike A1 excitation exhibits characteristic softening and linewidth narrowing upon cooling toward $T^*$, while retaining substantial residual energy even as $T \to T^*$. The subsequent partial hardening and narrowing are interpreted as vestigial signatures of an amplitude (Higgs) mode associated with a exciton condensation. Strikingly, this mode is enhanced in the $B_{3g}$ channel, consistent with theoretical predictions [23,47,48]. The presence of weak signatures in the symmetry-forbidden $A_g$ channel is ascribed to the multiband character of the condensate or hybridization of the amplitude mode with the interband continuum.

In $Ta_2Pd_3Te_5$, we identify several deviations from the ideal excitonic insulator scenario. In particular, the order-parameter-like increase of the A1 excitation below $T^*$ is small compared to the large softening and linewidth narrowing observed above $T^*$ and the A1 excitation retains a quite broad spectral profile. This suggests that a genuine U(1) symmetry breaking is impeded by coupling of the excitonic order to the lattice and interband transitions. This coupling induces Landau damping, causing the amplitude mode to decay into electron-hole pairs and shortening the excitation lifetime [49]. Additionally, the mode's coherence is further destroyed by scattering from impurities, phonons, and electron-electron interactions. This collision-dominated mechanism is evidenced by the prominent low-frequency Drude-like response. Notwithstanding these dampings, the spectral features characteristic of an amplitude mode survive in a vestigial form.

In summary, our comprehensive Raman scattering study of $Ta_2Pd_3Te_5$ reveals correlation-driven excitonic condensation in the presence of subtle lattice symmetry breaking. The detection of collective amplitudelike modes, their symmetry

selectivity, and their anisotropic coupling to the electronic background provide compelling spectroscopic evidence of excitonic order. These findings underscore the complex, multiband nature of excitonic insulators in real materials.

## ACKNOWLEDGMENTS

The work at SKKU was supported by the National Research Foundation (NRF) of Korea (Grants No. RS-2023-00209121 and No. 2020R1A5A1016518). R.S. acknowledges the financial support provided by the Ministry of Science and Technology in Taiwan under Projects No. 114-2124-M-001-009 and No. NSTC-114-2112M001-045-MY3, as well as support from Academia Sinica for the budget of ASiMATE115-14 and financial support from the Center of Atomic Initiative for New Materials (AIMat), National Taiwan University, under Project No. 115L900801. R.K.U. would like to acknowledge the IITR for the Faculty Initiation Grant (No. FIG-101068). Y.-S.C. acknowledges the support from the NRF of Korea (Grant No. RS-2023-00214312). D.W. acknowledges support from the Institute of Applied Physics of Seoul National University, from the ITRC Program through the IITP, and from the Global Research Development Center (GRDC) Cooperative Hub Program through the NRF, funded by the (MSIT) (Grants No. RS-2024-00437191 and No. RS-2023-00258359).

## DATA AVAILABILITY

There are no publicly available research data or software supporting this manuscript. Requests for further information or data should be sent to the authors.

[1] T. Kaneko and Y. Ohta, A new era of excitonic insulators, J. Phys. Soc. Jpn. **94**, 012001 (2025).
[2] N. F. Mott, The transition to the metallic state, Philos. Mag. **6**, 287 (1961).
[3] L. V. Keldysh and Y. V. Kopeav, Possible instability of the semimetallic state toward Coulomb interaction, Sov. Phys. Solid State **6**, 2219 (1965).
[4] J. D. Cloizeaux, Exciton instability and crystallographic anomalies in semiconductors, J. Phys. Chem. Solids **26**, 259 (1965).
[5] W. Kohn, Excitonic phases, Phys. Rev. Lett. **19**, 439 (1967).
[6] J. Zittartz, Theory of the excitonic insulator in the presence of normal impurities, Phys. Rev. **164**, 575 (1967).
[7] D. Jerome, T. M. Rice, and W. Kohn, Excitonic insulator, Phys. Rev. **158**, 462 (1967).
[8] B. I. Halperin and T. M. Rice, Possible anomalies at a semimetal-semiconductor transistion, Rev. Mod. Phys. **40**, 755 (1968).
[9] J. Kuneš, Excitonic condensation in systems of strongly correlated electrons, J. Phys.: Condens. Matter **27**, 333201 (2015).
[10] M. M. Traum, G. Margaritondo, N. V. Smith, J. E. Rowe, and F. J. Di Salvo, $TiSe_2$: Semiconductor, semimetal, or excitonic insulator, Phys. Rev. B **17**, 1836 (1978).
[11] A. Kogar, M. S. Rak, S. Vig, A. A. Husain, F. Flicker, Y. I. Joe, L. Venema, G. J. MacDougall, T. C. Chiang, E. Fradkin, J. van Wezel, and P. Abbamonte, Signatures of exciton condensation in a transition metal dichalcogenide, Science **358**, 1314 (2017).
[12] T. Pillo, J. Hayoz, H. Berger, F. Lévy, L. Schlapbach, and P. Aebi, Photoemission of bands above the Fermi level: The excitonic insulator phase transition in $1T-TiSe_2$, Phys. Rev. B **61**, 16213 (2000).
[13] H. Cercellier, C. Monney, F. Clerc, C. Battaglia, L. Despont, M. G. Garnier, H. Beck, P. Aebi, L. Patthey, H. Berger, and L. Forró, Evidence for an excitonic insulator phase in $1T-TiSe_2$, Phys. Rev. Lett. **99**, 146403 (2007).
[14] C. Monney, C. Battaglia, H. Cercellier, P. Aebi, and H. Beck, Exciton condensation driving the periodic lattice distortion of $1T-TiSe_2$, Phys. Rev. Lett. **106**, 106404 (2011).
[15] H. Hedayat, C. J. Sayers, D. Bugini, C. Dallera, D. Wolverson, T. Batten, S. Karbassi, S. Friedemann, G. Cerullo, J. van Wezel, S. R. Clark, E. Carpene, and E. Da Como, Excitonic and lattice contributions to the charge density wave in $1T-TiSe_2$ revealed by a phonon bottleneck, Phys. Rev. Res. **1**, 023029 (2019).
[16] S. A. Sunshine and J. A. Ibers, Structure and physical properties of the new layered ternary chalcogenides tantalum nickel sulfide ($Ta_2NiS_5$) and tantalum nickel selenide ($Ta_2NiSe_5$), Inorg. Chem. **24**, 3611 (1985).
[17] Y. Wakisaka, T. Sudayama, K. Takubo, T. Mizokawa, M. Arita, H. Namatame, M. Taniguchi, N. Katayama, M. Nohara, and H. Takagi, Excitonic insulator state in $Ta_2NiSe_5$ probed by photoemission spectroscopy, Phys. Rev. Lett. **103**, 026402 (2009).
[18] K. Seki, Y. Wakisaka, T. Kaneko, T. Toriyama, T. Konishi, T. Sudayama, N. L. Saini, M. Arita, H. Namatame, M. Taniguchi, N. Katayama, M. Nohara, H. Takagi, T. Mizokawa, and Y. Ohta, Excitonic Bose-Einstein condensation in $Ta_2NiSe_5$ above room temperature, Phys. Rev. B **90**, 155116 (2014).
[19] Y. F. Lu, H. Kono, T. I. Larkin, A. W. Rost, T. Takayama, A. V. Boris, B. Keimer, and H. Takagi, Zero-gap semiconductor to excitonic insulator transition in $Ta_2NiSe_5$, Nat. Commun. **8**, 14408 (2017).
[20] T. I. Larkin, A. N. Yaresko, D. Pröpper, K. A. Kikoin, Y. F. Lu, T. Takayama, Y.-L. Mathis, A. Rost, H. Takagi, B. Keimer, *et al.*, Giant exciton Fano resonance in quasi-one-dimensional $Ta_2NiSe_5$, Phys. Rev. B **95**, 195144 (2017).
[21] S. Mor, M. Herzog, J. Noack, N. Katayama, M. Nohara, H. Takagi, A. Trunschke, T. Mizokawa, C. Monney, and J. Stähler, Inhibition of the photoinduced structural phase transition in the excitonic insulator $Ta_2NiSe_5$, Phys. Rev. B **97**, 115154 (2018).
[22] K. Sugimoto, S. Nishimoto, T. Kaneko, and Y. Ohta, Strong coupling nature of the excitonic insulator state in $Ta_2NiSe_5$, Phys. Rev. Lett. **120**, 247602 (2018).
[23] G. Mazza, M. Rösner, L. Windgätter, S. Latini, H. Hübener, A. J. Millis, A. Rubio, and A. Georges, Nature of symmetry breaking at the excitonic insulator transition: $Ta_2NiSe_5$, Phys. Rev. Lett. **124**, 197601 (2020).
[24] H. M. Bretscher, P. Andrich, Y. Murakami, D. Golež, B. Remez, P. Telang, A. Singh, L. Harnagea, N. R. Cooper, A. J. Millis, P.

Werner, A. K. Sood, and A. Rao, Imaging the coherent propagation of collective modes in the excitonic insulator $Ta_2NiSe_5$ at room temperature, Sci. Adv. **7**, eabd6147 (2021).

[25] K. Kim, H. Kim, J. Kim, C. Kwon, J. S. Kim, and B. J. Kim, Direct observation of excitonic instability in $Ta_2NiSe_5$, Nat. Commun. **12**, 1969 (2021).

[26] K. Fukutani, R. Stania, C. I. Kwon, J. S. Kim, K. J. Kong, J. Kim, and H. W. Yeom, Detecting photoelectrons from spontaneously formed excitons, Nat. Phys. **17**, 1024 (2021).

[27] E. Baldini, A. Zong, D. Choi, C. Lee, M. H. Michael, L. Windgaetter, I. I. Mazin, S. Latini, D. Azoury, B. Lv, A. Kogar, Y. Su, Y. Wang, Y. Lu, T. Takayama, H. Takagi, A. J. Millis, A. Rubio, E. Demler, and N. Gedik, The spontaneous symmetry breaking in $Ta_2NiSe_5$ is structural in nature, Proc. Natl. Acad. Sci. USA **120**, e2221688120 (2023).

[28] K. Katsumi, A. Alekhin, S.-M. Souliou, M. Merz, A.-A. Haghighirad, M. L. Tacon, S. Houver, M. Cazayous, A. Sacuto, and Y. Gallais, Disentangling lattice and electronic instabilities in the excitonic insulator candidate $Ta_2NiSe_5$ by nonequilibrium spectroscopy, Phys. Rev. Lett. **130**, 106904 (2023).

[29] Z. Guo, D. Yan, H. Sheng, S. Nie, Y. Shi, and Z. Wang, Quantum spin Hall effect in $Ta_2M_3Te_5$ (M = Pd, Ni), Phys. Rev. B **103**, 115145 (2021).

[30] Z. Guo, J. Deng, Y. Xie, and Z. Wang, Quadrupole topological insulators in $Ta_2M_3Te_5$ (M = Ni, Pd) monolayers, npj Quantum Mater, **7**, 87 (2022).

[31] J. Yao, H. Sheng, R. Zhang, R. Pang, J.-J. Zhou, Q. Wu, H. Weng, X. Dai, Z. Fang, and Z. Wang, Excitonic instability in $Ta_2Pd_3Te_5$ monolayer, Chin. Phys. Lett. **41**, 097101 (2024).

[32] X. Wang, D. Geng, D. Yan, W. Hu, H. Zhang, S. Yue, Z. Sun, S. Kumar, E. F. Schwier, K. Shimada, P. Cheng, L. Chen, S. Nie, Z. Wang, Y. Shi, Y.-Q. Zhang, K. Wu, and B. Feng, Observation of topological edge states in the quantum spin Hall insulator $Ta_2Pd_3Te_5$, Phys. Rev. B **104**, L241408 (2021).

[33] A. Wang, Y. Li, G. Yang, D. Yan, Y. Huang, Z. Guo, J. Gao, J. Huang, Q. Zeng, D. Qian, *et al.*, A robust and tunable Luttinger liquid in correlated edge of transition-metal second-order topological insulator $Ta_2Pd_3Te_5$, Nat. Commun. **14**, 7647 (2023).

[34] Y. Li, D. Yan, Y. Hong, H. Sheng, A. Wang, Z. Dou, X. Guo, X. Shi, Z. Su, Z. Lyu, T. Qian, G. Liu, F. Qu, K. Jiang, Z. Wang, Y. Shi, Z.-A. Xu, J. Hu, L. Lu, and J. Shen, Interfering Josephson diode effect in $TaPd_3Te_5$ asymmetric edge interferometer, Nat. Commun. **15**, 9031 (2024).

[35] H. Yu, D. Yan, Z. Guo, Y. Zhou, X. Yang, P. Li, Z. Wang, X. Xiang, J. Li, X. Ma, *et al.*, Observation of emergent superconductivity in the topological insulator $Ta_2Pd_3Te_5$ via pressure manipulation, J. Am. Chem. Soc. **146**, 3890 (2024).

[36] Z. Sun, Z. Guo, D. Yan, P. Cheng, L. Chen, Y. Shi, Y. Huang, Z. Wang, K. Wu, and B. Feng, Layer-dependent Raman spectroscopy of ultrathin $Ta_2Pd_3Te_5$, Phys. Rev. Mater. **7**, 094004 (2023).

[37] J. Huang, B. Jiang, J. Yao, D. Yan, X. Lei, J. Gao, Z. Guo, F. Jin, Y. Li, Z. Yuan, *et al.*, Evidence for an excitonic insulator state in $Ta_2Pd_3Te_5$, Phys. Rev. X **14**, 011046 (2024).

[38] P. Zhang, Y. Dong, D. Yan, B. Jiang, T. Yang, J. Li, Z. Guo, Y. Huang, Haobo, Q. Li, *et al.*, Spontaneous gap opening and potential excitonic states in an ideal Dirac semimetal $Ta_2Pd_3Te_5$, Phys. Rev. X **14**, 011047 (2024).

[39] M. S. Hossain, T. A. Cochran, Y.-X. Jiang, S. Zhang, H. Wu, X. Liu, X. Zheng, B. Kim, G. Cheng, Q. Zhang, *et al.*, Topological excitonic insulator with tunable momentum order, Nat. Phys. **21**, 1250 (2025).

[40] G. Mazza, Intertwined orders in a quantum material, Nat. Phys. **21**, 1181 (2025).

[41] S. Lee, K.-H. Jin, S. J. Kwon, H. Jung, C. Won, S.-W. Cheong, G. Y. Cho, J. Kim, and H. W. Yeom, Exciton photoemission from a ground state of a solid $Ta_2Pd_3Te_5$, Phys. Rev. Lett. **135**, 116401 (2025).

[42] See Supplemental Material at http://link.aps.org/supplemental/10.1103/2swg-p1pn for (1) complete phonon mode assignments, (2) angular dependence of Raman intensity of $A_g$ phonon modes, and (3) temperature dependence of phonon modes, which includes Ref. [36].

[43] M. V. Klein, Electronic Raman scattering, in *Light Scattering in Solids I*, edited by M. Cardona, Topics in Applied Physics (Springer, Berlin, 1983), Vol. 8.

[44] P. Lemmens, K. Y. Choi, V. Gnezdilov, E. Y. Sherman, D. P. Chen, C. T. Lin, F. C. Chou, and B. Keimer, Anomalous electronic Raman scattering in $Na_xCoO_2 \cdot yH_2O$, Phys. Rev. Lett. **96**, 167204 (2006).

[45] S. Yi, Z. Liao, C. Liang, S. Zhang, X. Deng, Y. Xie, L. Zheng, Y. Wang, Y. Wu, Z. Wang, Y. Shi, X. Qiu, and B. Xu, Optical excitations of flat bands induced by exciton condensation in $Ta_2Pd_3Te_5$, arXiv:2506.18350.

[46] P. A. Volkov, M. Ye, H. Lohani, I. Feldman, A. Kanigel, and G. Blumberg, Critical charge fluctuations and emergent coherence in a strongly correlated excitonic insulator, npj Quantum Mater. **6**, 52 (2021).

[47] Y. Murakami, D. Golež, T. Kaneko, A. Koga, A. J. Millis, and P. Werner, Collective modes in excitonic insulators: Effects of electron-phonon coupling and signatures in the optical response, Phys. Rev. B **101**, 195118 (2020).

[48] B. Chatterjee, J. Mravlje, and D. Golež, Collective modes and Raman response in $Ta_2NiSe_5$, Phys. Rev. B **111**, L121106 (2025).

[49] H. C. Lee and H. Y. Cho, Electronic Raman scattering of two-band superconductors: A time-dependent Landau–Ginzburg theory approach, J. Phys.: Condens. Matter **21**, 445701 (2009).

*Correction:* The second affiliation contained errors and has been fixed.